Journal of the Korean Nuclear Society
Volume 31, Number 4, pp.432~443, August 1999

Two-Dimensional Nuclide Transport Around a HLW Repository

Youn-Myoung Lee, Chul-Hyung Kang, Yong Soo Hwang, and Kwan-Sik Chun
Korea Atomic Energy Research Institute
150 Dukjin-dong, Yusong-gu, Taejon, 305-353, Korea
ymlee@kaeri.re.kr

(Received April 28, 1999)

Abstract

Using a two-dimensional numerical model, nuclide transport in the buffer between the canister and adjacent rock in a high-level radioactive waste repository is dealt with. Calculations are made for a typical case with a three-member decay chain, $^{234}U \rightarrow {}^{230}Th \rightarrow {}^{226}Ra$. The solution method used here is based on a physically exact formulation by a control volume method directly integrating the governing equation over each control volume.

Key Words : nuclide transport, chain decay, two-dimensional model, HLW repository

Notation

$2b$ = fracture aperture, [L]
b = super- and subscripts denoting the buffer
b,p = super- and subscripts denoting the buffer or matrix
$\tilde{c}_l(t)$ = concentration of nuclide l at the inlet, [ML^{-3}]
$\tilde{c}_E, c_W, c_N, c_S, c_P$ = concentrations at each grid point as shown in Figs. 3 and 4, [ML^{-3}]
c_l = concentration of nuclide l, [ML^{-3}]
c_l^0 = initial concentration of nuclide l at the inlet, [ML^{-3}]
D^* = molecular diffusion coefficient in water, [L^{2}T^{-1}]
$D_{b\rightarrow f}$ = interface diffusion coefficient through the buffer-fracture interface as defined in Eq. (A15), [L^{2}T^{-1}]
$D_{b\rightarrow p}$ = interface diffusion coefficient through the buffer-matrix interface as defined in Eq. (A14), [L^{2}T^{-1}]
$D_{f\rightarrow p}$ = interface diffusion coefficient through the fracture wall between the fracture and the matrix as defined in Eq. (A13), [L^{2}T^{-1}]
D_L = longitudinal hydrodynamic dispersion coefficient in the fracture, further expressed as $D_L = \alpha_L \cdot v + D^*$, [L^{2}T^{-1}]
$(D_L)_n$ = longitudinal hydrodynamic dispersion coefficient through control volume face n, [L^{2}T^{-1}]
$(D_L)_s$ = longitudinal hydrodynamic dispersion coefficient through control volume face s, [L^{2}T^{-1}]
D_T = transverse hydrodynamic dispersion coefficient in the fracture, [L^{2}T^{-1}]
e, w, n, s = control volume faces as defined in

Figs. 3 and 4

E, W, N, S, P = subscripts for grid point concentration as shown in Figs. 3 and 4

J = total flux in the fracture as defined in Eq. (A1), [$ML^{-2}T^{-1}$]

K_d^l = distribution coefficient for nuclide l, [L^3M^{-1}]

l = subscript denoting parent nuclide

l-1 = subscript denoting daughter nuclide

p = super- and subscripts denoting the matrix

R_l = retardation coefficient in the fracture for nuclide l

R_l^b = retardation coefficient in the buffer for nuclide l

R_l^p = retardation coefficient in the matrix for nuclide l

t = elapsed time, [T]

$t_{0.5}$ = half-life of nuclide, [T]

v = groundwater velocity in the fracture, [LT^{-1}]

x, y = coordinates as defined in Fig. 1, [L]

x_m = half of fracture spacing (see Fig. 2), [L]

y_b = distance to the buffer-rock boundary (buffer thickness), [L]

y_m = distance to the outlet boundary, [L]

α_L = dispersivity along the fracture, [L]

$(\delta x)_e$, $(\delta x)_w$, $(\delta y)_s$, $(\delta y)_n$ = distance between nodes as defined in Fig. 4(b), [L]

$(\delta x)_{e+}$ = distance as defined in Fig. 4(b), [L]

Δx_i = spatial discretization increment in the x direction, [L]

Δt = temporal increment, [T]

Δy_j = spatial discretization increment in the y direction, [L]

λ_l = decay constant of nuclide l, [T^{-1}]

θ_b = porosity of the buffer

θ_p = porosity of the matrix

$(\theta_b D_x^b)$, $(\theta_b D_y^b)$ = effective diffusion coefficient in the buffer in the x and y directions, respectively, [L^2T^{-1}]

$(\theta_p D_x^p)$, $(\theta_p D_y^p)$ = effective diffusion coefficient in the matrix in the x and y directions, respectively, [L^2T^{-1}]

1. Introduction

In Korea, like many other countries, the potential repository for the final disposal of high-level radioactive waste (HLW) is to be located in deep geological formation. The disposal concept for the repository would be similar to that considered for Swedish KBS-3 (1983) concept in which the disposal of spent fuel assemblies in canisters individually emplaced in vertical deposition holes is considered. The buffer material should be designed for low permeability to delay the contact of the waste by groundwater, for strong sorption to retard or to delay the release of nuclides to such geologic media as host rocks. Therefore it is important to study the nuclide release through the buffer material into the rock for the repository assessment. For HLW repository located in deep geological formations, behavior of chain decaying nuclide in geological media has been an important topic in assessing its performance.

However, unfortunately, only a limited number of analytical works for limited modeling system are available relating the multi-member chain decay transport. Recently a series of studies associated with chain decay transport have been done numerically by authors (Lee et al., 1993; Lee et al., 1995; Lee and Lee, 1995; Lee et al, 1996; Lee and Kang, 1997; Lee et al, 1997).

The purpose of this paper is to show how nuclides can be transported across the buffer-matrix and buffer-fracture interfaces. This work presents an illustrative case of the two-dimensional finite-difference numerical solution for nuclide transport of an 'arbitrary decay chain length' (i.e., multi-member chain decay) through a buffer and a fractured porous medium in the vicinity of HLW repository by utilizing a control volume method, which is introduced in detail in previous work. (Lee and Kang, 1999)

2. Conceptual Model

Nuclides escaped from a penetrated canister will diffuse through the buffer material eventually to the host rock. Fractures in the host rock of a geological repository around the canister may intersect disposal holes for canister, providing advective pathways for the hydrogeologic nuclide transport, whereas porous rock matrix inerfaced with buffer will provide diffusive transport pathways for nuclides. Since fractures having permeabilities several orders of magnitude higher than the rock matrix itself provide a main hydrogeologic pathway for the transport of the nuclide into the far-field region, the assumption that the rock matrix surrounding the buffer is impervious to nuclide transport has commonly been made. However, recently, studies show that the nuclides are available to diffuse freely across the buffer-matrix boundary.

Such an approach is difficult to be handled with an analytical method due to the complexity of domain.

The physical system of the fractured rock modeled here is similar to that treated in many works (e.g., Sudicky and Frind, 1982; Sudicky and Frind, 1984; Lee et al., 1989; Lee et al., 1993; Lee and Lee, 1995; Lee and Kang, 1997). In these models thin rigid parallel fractures are embedded in a saturated porous rock matrix. The buffer is modeled as a two-dimensional porous medium as shown in Fig. 1. The planar geometry of the modeled domain is shown in Fig. 2.

If a linear sorption isotherm is assumed, transport for the nuclide l in a saturated fracture is commonly described by

$$R_l\frac{\partial c_l}{\partial t}+\lambda_l c_l R_l=\frac{\partial}{\partial x}\left(D_T\frac{\partial c_l}{\partial x}\right)+\frac{\partial}{\partial y}\left(D_L\frac{\partial c_l}{\partial y}-vc_l\right)+\lambda_{l-1}c_{l-1}R_{l-1},\quad 0<x<b,\ y_b<y<y_m,\ t>0. \tag{1}$$

Also, assuming that there is no advective transport in the buffer as well as in the matrix at all, the governing equation is

$$R_l^{b,p}\frac{\partial c_l}{\partial t}+\lambda_l c_l R_l^{b,p}=\frac{\partial}{\partial x}\left(\theta_{b,p}D_x^{b,p}\frac{\partial c_l}{\partial x}\right)+\frac{\partial}{\partial y}\left(\theta_{b,p}D_y^{b,p}\frac{\partial c_l}{\partial y}\right)+\lambda_{l-1}c_{l-1}R_{l-1}^{b,p},\quad \begin{cases}0<x<x_m, 0<y<y_b, t>0; & \text{for bufffer}\\ b<x<x_m, y_b<y<y_m, t>0; & \text{for matrix.}\end{cases} \tag{2}$$

The discretized domain for the buffer and fractured porous media is as depicted in Fig. 3, where the boundary conditions are zero concentration gradient (Neuman-type) boundary conditions, at all boundaries except at the canister surface interface.

$$\frac{\partial c_l}{\partial x}=0,\quad x=0, x=x_m; \tag{3a}$$

at the centers of the fracture and the matrix between two parallel fractures,

$$\frac{\partial c_l}{\partial y}=0;\quad y=y_m; \tag{3b}$$

at the outlet of the modeled domain.

For initial and boundary conditions associated with the inlet of the buffer, nuclide decay and transformation of the parent nuclide into its daughter products are considered together by Bateman' s decaying source. The concentration at the inlet boundary for the l-th component of the decay chain, $\tilde{c}_l(t)$, which is written as

$$\tilde{c}_l(t)=\sum_{m=1}^{l}B_{lm}e^{-\lambda_m t} \tag{4a}$$

where

$$B_{lm}=\sum_{n=1}^{m}c_n^0\prod_{k=n}^{l-1}\lambda_k\left\{\prod_{\substack{j=n\\ j\neq m}}^{l}(\lambda_j-\lambda_m)\right\}^{-1} \tag{4b}$$

and c_l^0 denotes the initial concentration at the inlet.

To derive a two-dimensional discretization equation by control volume approach, first of all, a grid-point cluster is introduced. (See Fig. 4.) The modeled domain is divided into variably sized control volumes, each of which has a central grid

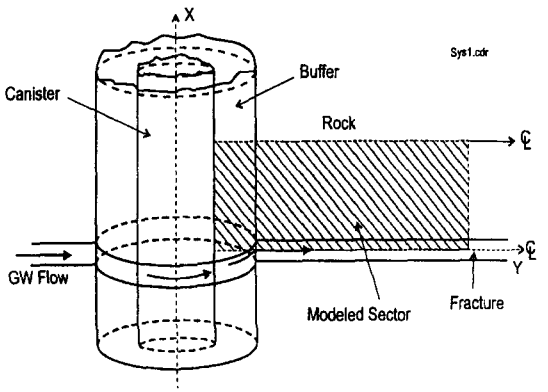

Fig. 1. Schematic View in the Vicinity of a Deposition Hole Intersected by a Fracture in a Potential HLW Repository

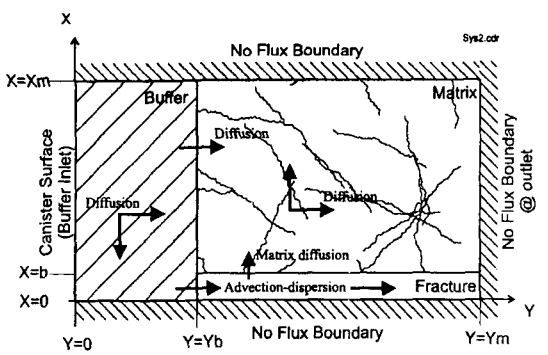

Fig. 2. The Planar Geometry Representation of the Modeled Domain

point located in the geometrical center of the control volume. The control volume faces are not necessarily located equidistant from the two adjacent nodes. Once the control volumes have been defined, the concentration value is evaluated at each node. The full description for the discretization procedure is represented in detail in Appendix I.

In order to avoid a discontinuity in physical properties within a control volume, discontinuities in the medium, such as at the

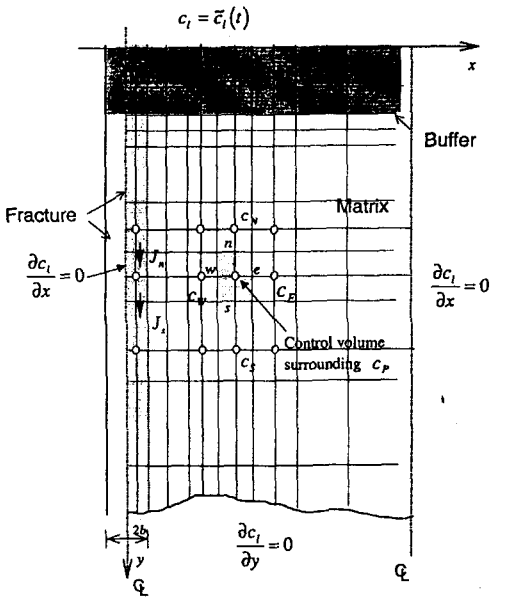

Fig. 3. Discretized Two-dimensional Domain for Buffer and the Fractured Medium

no flux boundary and the fracture-matrix boundary, are recommended to be located at control volume faces. Although it leads to the half-sized control volumes around the grid points, by postulating a grid point at the face having control volume of zero thickness, the need for special discretization at discontinuities can be eliminated.

The solutions of the algebraic equations (A9) and (A11) are then obtained using a simple Gauss-Seidel iteration scheme.

To deal with interface diffusion coefficients, $D_{f\to p}$, $D_{b\to p}$, and $D_{b\to f}$ when the diffusion coefficients or dispersion coefficients are different in adjacent control volumes as in such cases as the fracture wall interfaced with the matrix and the buffer interfaced with rock, the analogy to a series of resistors can be utilized in the same way as discussed by Patankar (1980). Detailed discussions are to be found in Appendix II.

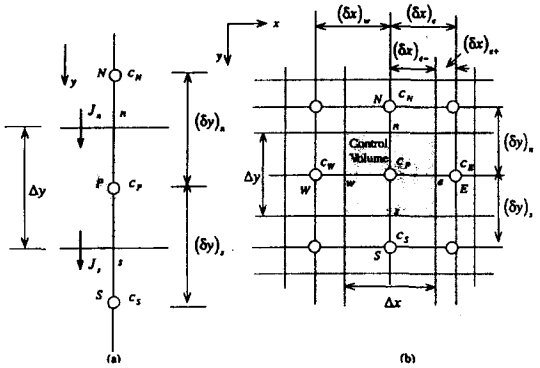

Fig. 4. (a) Steady State One-dimensional Consideration for the Flux in the Fracture; (b) Two-dimensional Control Volumes in the Matrix and the Fracture

3. Numerical Illustration

To illustrate an application of the numerical technique, the decay chain $^{234}U \rightarrow ^{230}Th \rightarrow ^{226}Ra$ which is one of the most important chains in HLW was chosen. It is emphasized that the solution and associated computer code are not limited by the number of members in the chain and that this three member decay chain was considered for simplicity. Parameters used are listed in Tables 1 and 2. As seen in the Table 3, the number of control volumes used is 20 in the x-direction into the matrix and 100 in the y-direction along the fracture axis, giving a total of 20 by 100 control volumes.

Figs. 5 to 7 show the concentration profiles normalized to the parent nuclide (^{234}U) concentration at the inlet boundary as a function of distance in the direction of the fracture, y at times equal to 4×10^2, 396,400, and 3,960,400 years, respectively. The concentration at the inlet, $\tilde{c}_1$, is changed by Bateman equation. With the advection-dispersion parameters chosen, these calculations show that ^{234}U travels faster than the other two nuclides, due to its smaller retardation and longer half-life.

For more effective calculation, varying temporal steps according to the calculation time can be used. After some numerical experiments, optimum temporal sizes are obtained. An acceptable time steps are listed in Table 4.

In these figures one can see all profiles are abruptly changed around at y=0.35m because there exists the buffer-rock boundary across which the properties of media are changed.

The profiles of ^{234}U, ^{230}Th and ^{226}Ra are shown at two fixed points of interest, i.e., $x=3\times10^{-5}$ m and $x=1.5\times10^{-2}$ m in the direction perpendicular to the fracture, corresponding to i=1 and i=10, respectively. These two points are intensionally

Table 1. Parameter Used

Parameter	Value
2_b	120 μm
θ_b	0.1
θ_p	0.4
α_L	0.76 m
υ	0.75 m/yr
D^*	10^{-7} m^2/yr
y_b	35 cm

Table 2. Input Data for Chain Transport

Nuclide	$t_{0.5}$, yr	R_l, R^b_l, R^p_l	c_l^0
^{234}U	2.47×10^5	120	c_0
^{230}Th	8×10^4	1500	0
^{226}Ra	1600	300	0

Table 3. Spatial Increments for the Control Volume (decay chain transport)

Δx_i, cm i = 1, 2, 3, ···, 20	0.006, 0.009, 0.015, 0.025, 0.045, 0.07, 0.13, 0.25, 0.45, 1(i=10~20)
Δy_j, cm j=1, 2, 3,···, 100	7 (j=1~5); for buffer, 10 (j=6~10), 15 (j=11~50), 20, (j=51~100); for fracture and matrix

Table 4. Temporal Sizes Used for Breakthrough Calculations

Time, yrs	Δt, yrs
$0 - 4 \times 10^1$	2×10^{-1}
$0 - 4 \times 10^3$	2×10^0
$0 - 1 \times 10^5$	2×10^1
1×10^5-	4×10^3

chosen to deal with two different component of media; the buffer-matrix and the buffer-fracture. The same values of retardation factors for each medium of the buffer, the matrix and the fracture are used for simplicity. The profiles show the same trend; higher concentration profiles in the buffer are changed to lower profiles in the matrix and lower profiles in the buffer are changed to higher profiles in the fracture on the contrary. This is because the nuclides entering the fracture are taken away by advection and dispersion due to groundwater flow takes place only in the fracture although there is a loss term due to matrix diffusion into the matrix from the fracture. Also, it should be noted that no flux boundary conditions are used at each side of the buffer, which results in fast profiles in the center of buffer media.

In Figs. 6 and 7, the concentrations of ^{230}Th and ^{226}Ra at $y = 10.15$ m (in rock medium; both in the fracture and the matrix) reveal that they are still rising and becoming flat, whereas the concentration of ^{234}U alone shows its peak values earlier in Fig. 6 (among three figures, Figs. 5 to 7) due to decay effect already started to take place. Note that the half-life of ^{234}U is 2.47×10^5 years.

However, the concentrations of all nuclides at y=1.75 m (in buffer medium) including ^{234}U show their peak concentrations in Fig. 6.

Two-dimensional concentration isopleths normalized to initial ^{234}U concentrations (c_0) for the above case are also plotted in Figs. 8 to 16 at times of 4×10^4, 396,400 and 3,960,400 years for ^{234}U, ^{230}Th, and ^{226}Ra. The plots commonly

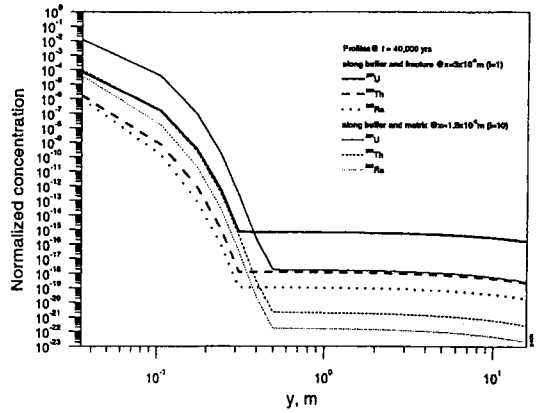

Fig. 5. Profiles at t = 40,000 Years

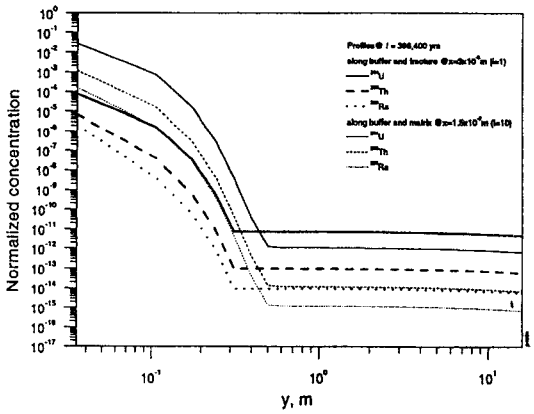

Fig. 6. Profiles at t = 396,400 Years

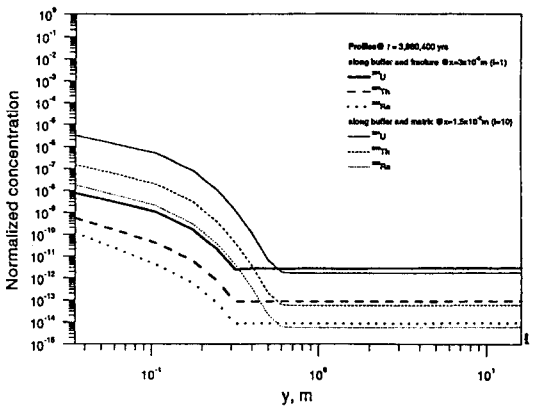

Fig. 7. Profiles at t = 3,960,400 Years

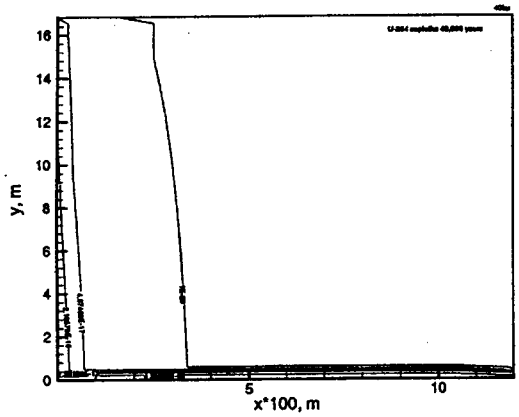

Fig. 8. Concentration Isopleths for ^{234}U at t = 40,000 Years

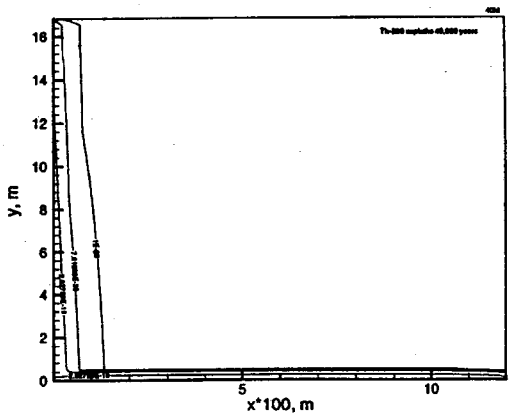

Fig. 9. Concentration Isopleths for ^{230}Th at t = 40,000 Years

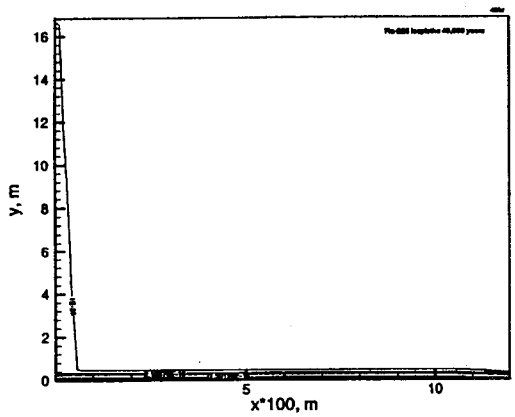

Fig. 10. Concentration isopleths for ^{226}Ra at t = 40,000 years

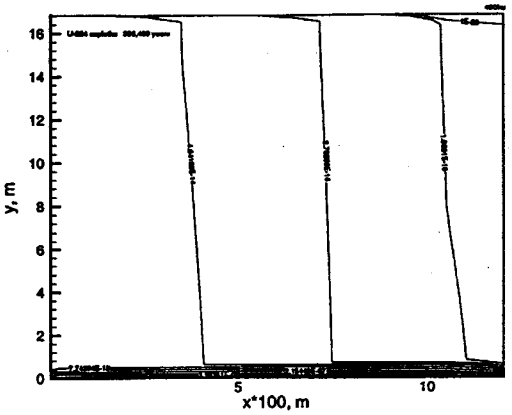

Fig. 11. Concentration Isopleths for ^{234}U at t = 396,400 Years

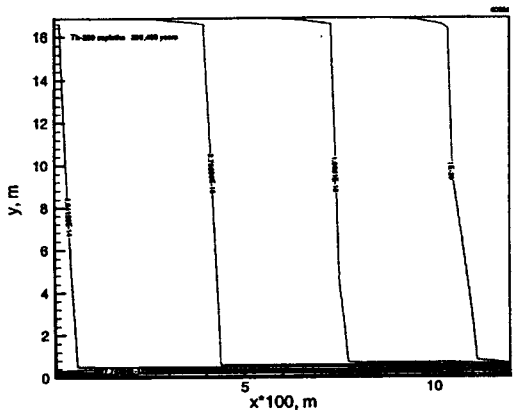

Fig. 12. Concentration Isopleths for ^{230}Th at t = 396,400 Years

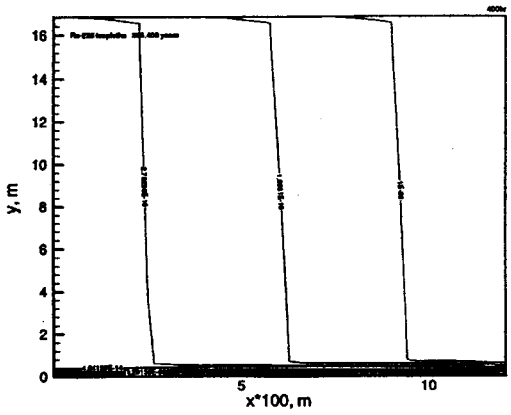

Fig. 13. Concentration Isopleths for ^{226}Ra at t = 396,400 Years

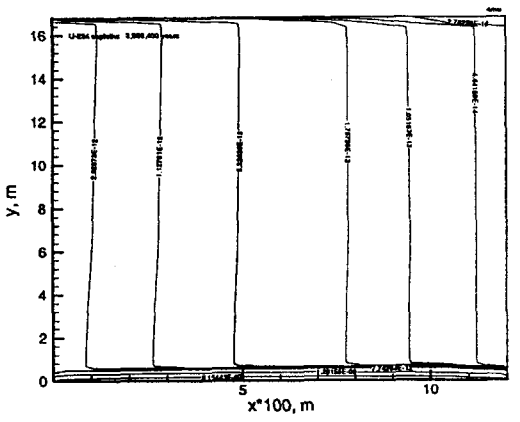

Fig. 14. Concentration Isopleths for ^{234}U at t = 3,960,400 Years

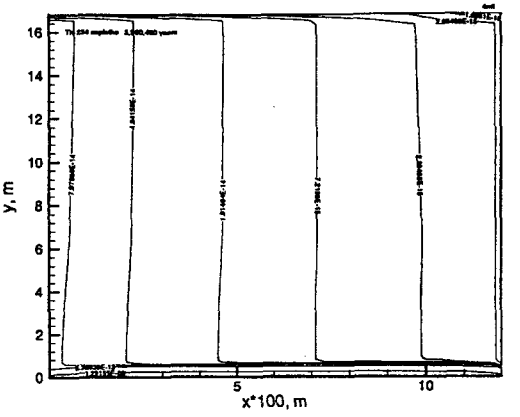

Fig. 15. Concentration Isopleths for ^{230}Th at t = 3,960,400 Years

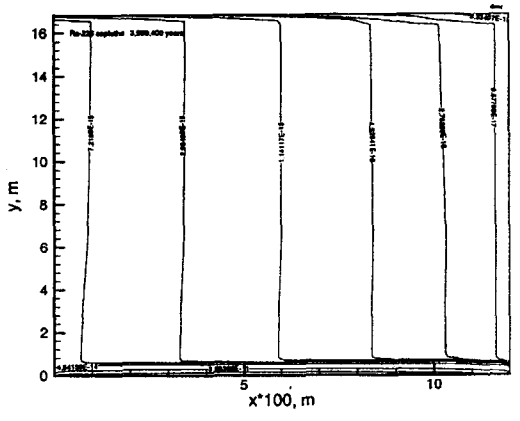

Fig. 16. Concentration Isopleths for ^{226}Ra at t = 3,960,400 Years

show that the plumes progress very gently at early times and then change abruptly in the vicinity of the buffer-rock interface.

Figs. 17 and 18 show the normalized concentration profiles as a function of time at distances y =0.245 and y =6.775 m. At these two distances each of which is rather randomly selected for the buffer and the rock, two sets of profiles seem to be similar showing the peak concentration around 10^6 years.

Initially there are no ^{230}Th and ^{226}Ra both in the source and in the field and all of these nuclides come from the decay of ^{234}U, which has a very long half-life of 2.47×10^5 years. Therefore one can expect the low concentrations of the daughter nuclides in the field at early times as shown in the figures.

Actually, Fig. 17 shows the concentration for the buffer medium only, whereas Fig. 18 shows the concentration for the buffer-rock media, where the interface exists at y=0.35m. Some unacceptable results happen to the curve of ^{234}U at early times, which may result from an abrupt change of temporal size, because of the use of the discrete values shown in Table 4.

4. Concluding Remarks

A numerical technique by a control volume method has been introduced for multi-member chain decay and transport through a fractured porous rock matrix in previous work. Also, in order to demonstrate and verify the model developed through the study, the concentrations for some typical cases have been compared with such semi-analytical solutions by Tang *et al.* (1981) and Chiou and Li (1993) which utilizes

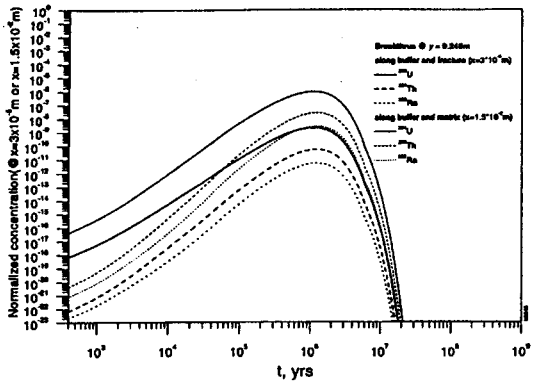

Fig. 17. Breakthroughs as a Function of Time at y = 0.245 m

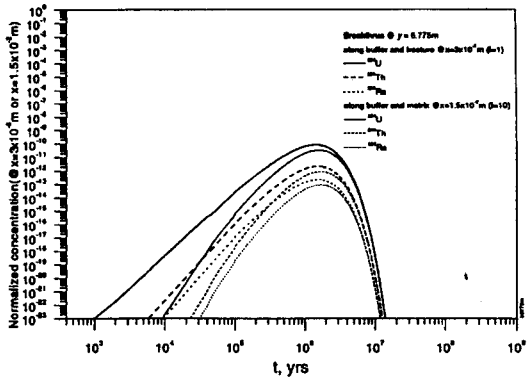

Fig. 18. Breakthroughs as a Function of Time at y = 6.775 m

Laplace transform and the inverse Laplace transform method proposed by Green (1955), respectively.

These comparison was made only indirectly because no exact solutions for multi-member chain decay and transport have been found yet, although solutions for limited case, e.g., for two-member decay chain by Sudicky and Frind (1984) is available. The comparison showed that the model through previous study generally agreed with exact solutions well although sometimes there showed some discrepancy. However, additional calculations with varying control volume dimensions show that if a smaller dimension is adopted the discrepancy could be dramatically reduced. In contrast, once the criterion for the appropriate temporal size has been found, the exactness of the solution does not seem to be very sensitive to the size of the temporal interval provided that it is less than the critical value.

In the present study, nuclide transport in the buffer surrounding the canister and rock medium has been considered by utilizing the two-dimensional numerical model developed through previous work. An illustrative case of the two-dimensional finite-difference numerical solution for nuclide transport of an arbitrary decay chain length through a buffer and a fractured porous medium in the vicinity of HLW repository, which may be of importance in view of performance of the repository. The three-member decay chain $^{234}U \rightarrow {}^{230}Th \rightarrow {}^{226}Ra$ is adopted in the numerical illustration.

Even though this model is based on a physically exact formulation utilizing a control volume method and then the differential governing equation is directly integrated over each control volume (and the model has already been partially verified in previous work), it may still need further comparison study with the exact solutions for the case with a matrix diffusion solution that involves chain decay in direct manner, as discussed through previous work.

Another distinct feature of the model developed in this paper is that it employs variable temporal and spatial discretization sizes, which makes it possible to address larger practical problems than with fixed discretization.

Appendix I. Two-Dimensional Discretization Equation

Designate the grid point in a control volume as P, with neighbors E and W in the x-direction and

S and N in the y-direction.

The control volume around P shown shaded in Fig. 4 has a volume of $1 \times \Delta x \times \Delta y$ with unit thickness of notional z-direction in a two-dimensional domain.

In order to avoid unrealistic results, it is convenient to consider the total flux due to advection plus dispersion in the fracture, utilizing an available analytical solution for the steady-state advection-dispersion equation, as introduced by Patankar (1980). This is called the exponential scheme.

Since the solution is obtained by marching forward in time, the discretization equations are derived by integrating Eqs. (1) and (2) over the control volume for node P and over the time interval Δt, which are represented as Eq. (A1) and (A2), respectively:

$$\int_w^e \int_s^n \int_t^{t+\Delta t} \left(R_i \frac{\partial c_i}{\partial t} + \lambda_i c_i R_i \right) dt\,dy\,dx = \int_w^e \int_s^n \int_t^{t+\Delta t} \left(\frac{\partial}{\partial x}\left\{ D_T \frac{\partial c_i}{\partial x} \right\} - \frac{\partial J}{\partial y} + \lambda_{i-1} c_{i-1} R_{i-1} \right) dt\,dy\,dx \tag{A1}$$

where J denotes the total flux, expressed as

$$J = v c_i - D_L \frac{\partial c_i}{\partial y}$$

$$\int_w^e \int_s^n \int_t^{t+\Delta t} \left(R_i^P \frac{\partial c_i}{\partial t} + \lambda_i c_i R_i^P \right) dt\,dy\,dx = \int_w^e \int_s^n \int_t^{t+\Delta t} \left(\frac{\partial}{\partial x}\left\{ (\theta D_x^P) \frac{\partial c_i}{\partial x} \right\} + \frac{\partial}{\partial y}\left\{ (\theta D_y^P) \frac{\partial c_i}{\partial y} \right\} + \lambda_{i-1} c_{i-1} R_{i-1}^P \right) dt\,dy\,dx. \tag{A2}$$

Eq. (A1) can be evaluated as

$$\Delta x \Delta y R_i \left\{ \left({}_i c_P^{t+\Delta t} - {}_i c_P^t \right) + \lambda_i {}_i c_P^{t+\Delta t} \Delta t \right\} = \Delta t \Delta y D_T \left[\frac{{}_i c_E^{t+\Delta t} - {}_i c_P^{t+\Delta t}}{(\delta x)_e} - \frac{{}_i c_P^{t+\Delta t} - {}_i c_W^{t+\Delta t}}{(\delta x)_w} \right] - \Delta t \Delta x \left(J_n - J_s \right) + \lambda_{i-1} R_{i-1} c_P^{t+\Delta t} \Delta x \Delta y \Delta t. \tag{A3}$$

Similarly, from Eq. (A2),

$$\Delta x \Delta y R_i^P \left\{ \left({}_i c_P^{t+\Delta t} - {}_i c_P^t \right) + \lambda_i {}_i c_P^{t+\Delta t} \Delta t \right\} = \Delta t \Delta y R_i^P \left(\theta D_x^P \right) \left[\frac{{}_i c_E^{t+\Delta t} - {}_i c_P^{t+\Delta t}}{(\delta x)_e} - \frac{{}_i c_P^{t+\Delta t} - {}_i c_W^{t+\Delta t}}{(\delta x)_w} \right] + \Delta t \Delta x R_i^P \left(\theta D_y^P \right) \left[\frac{{}_i c_N^{t+\Delta t} - {}_i c_P^{t+\Delta t}}{(\delta y)_n} - \frac{{}_i c_P^{t+\Delta t} - {}_i c_S^{t+\Delta t}}{(\delta x)_s} \right] + \lambda_{i-1} R_{i-1}^P {}_{i-1} c_P^{t+\Delta t} \Delta x \Delta y \Delta t. \tag{A4}$$

Meanwhile, the governing equation for a steady state one-dimensional case in which the advection and dispersion terms are dealt with could be generally represented as

$$v \frac{dc}{dy} - \frac{d}{dy}\left(D_L \frac{d}{dy} \right) = \frac{dJ}{dy} = 0 \tag{A5}$$

which has an exact solution for a domain $N \le y \le P$ (Fig. 4(a)) subject to $c(0)=c_N$ and $c(y=(\delta y)_n)=c_P$ as

$$c(y) = c_N + (c_P - c_N) \times \left\{ \frac{\exp(vy / D_L) - 1}{\exp\left[v(\delta y)_n / D_L \right] - 1} \right\} \tag{A6}$$

which leads to the flux through the face n of the control volume having a grid point P

$$J_n = vc - D_L \frac{\partial c}{\partial y} = vc_N + \frac{v(c_N - c_P)}{\exp\left[v(\delta y)_n / (D_L)_n \right] - 1}. \tag{A7}$$

Similarly, for the flux through the face s,

$$J_s = vc - D_L \frac{\partial c}{\partial y} = vc_P + \frac{v(c_P - c_S)}{\exp\left[v(\delta y)_s / (D_L)_s \right] - 1}. \tag{A8}$$

Then by introducing Eqs. (A7) and (A8) into Eq. (A3) would give

$$a_P^i {}_i c_P^{t+\Delta t} = a_E^i {}_i c_E^{t+\Delta t} + a_W^i {}_i c_W^{t+\Delta t} + a_N^i {}_i c_N^{t+\Delta t} + a_S^i {}_i c_S^{t+\Delta t} + d_i + \left\{ \left(\frac{R_{i-1}}{R_i} \right) \lambda_{i-1} \Delta x \Delta y \Delta t \right\}_{i-1} c_P^{t+\Delta t} \tag{A9}$$

where

$$a_P^i = \Delta x \Delta y + \Delta t \Delta y \frac{D_T}{R_i} \left\{ \frac{1}{(\delta x)_e} + \frac{1}{(\delta x)_w} \right\} + \frac{v}{R_i} \Delta x \Delta t \left\{ 1 + \frac{1}{\exp\left[v(\delta y)_n / (D_L)_n \right] - 1} + \frac{1}{\exp\left[v(\delta y)_s / (D_L)_s \right] - 1} \right\} + \lambda_i \Delta x \Delta y \Delta t, \tag{A10a}$$

$$a_E^i = \frac{\Delta t \Delta y D_T}{(\delta x)_e R_i}, \tag{A10b}$$

$$a_W^i = \frac{\Delta t \Delta y D_T}{(\delta x)_w R_i}, \tag{A10c}$$

$$a_S^i = \frac{v \Delta x \Delta t / R_i}{\exp\left[v(\delta y)_s / (D_L)_s \right] - 1}, \tag{A10d}$$

$$a_N^i = \frac{v}{R_i} \Delta x \Delta t \left(1 + \frac{1}{\exp\left[v(\delta y)_n / (D_L)_n \right] - 1} \right), \tag{A10e}$$

$$d_i = {}_i c_P^t \Delta x \Delta y. \tag{A10f}$$

Similarly, Eq. (A4) yields Eq. (A11).

$$a_{p,l}^{l}c_{p}^{t+\Delta t}=a_{e,l}^{l}c_{e}^{t+\Delta t}+a_{w,l}^{l}c_{w}^{t+\Delta t}+a_{n,l}^{l}c_{n}^{t+\Delta t}+a_{s,l}^{l}c_{s}^{t+\Delta t}+d_{l}+\left\{\left(\frac{R_{l-1}^{b,p}}{R_{l}^{b,p}}\right)\lambda_{l-1}\Delta x\Delta y\Delta z\right\}_{l-1}c_{b,p}^{t+\Delta t} \quad \text{(A11)}$$

where'

$$a_{p}^{l}=\theta_{b,p}\Delta x\Delta y+\Delta t\Delta y\frac{\left(\theta_{b,p}D_{x}^{b,p}\right)}{R_{l}^{b,p}}\left\{\frac{1}{(\delta x)_{e}}+\frac{1}{(\delta x)_{w}}\right\}\cdot+\Delta t\Delta x\frac{\left(\theta_{b,p}D_{y}^{b,p}\right)}{R_{l}^{b,p}}\left\{\frac{1}{(\delta y)_{n}}+\frac{1}{(\delta y)_{s}}\right\}+\lambda_{l}\theta_{b,p}\Delta x\Delta y, \quad \text{(A12a)}$$

$$a_{e}^{l}=\frac{\Delta t\Delta y\left(\theta_{b,p}D_{x}^{b,p}\right)/R_{l}^{b,p}}{(\delta x)_{e}}, \quad \text{(A12b)}$$

$$a_{w}^{l}=\frac{\Delta t\Delta y\left(\theta_{b,p}D_{x}^{b,p}\right)/R_{l}^{b,p}}{(\delta x)_{w}}, \quad \text{(A12c)}$$

$$a_{s}^{l}=\frac{\Delta t\Delta x\left(\theta_{b,p}D_{y}^{b,p}\right)/R_{l}^{b,p}}{(\delta y)_{s}}, \quad \text{(A12d)}$$

$$a_{n}^{l}=\frac{\Delta t\Delta x\left(\theta_{b,p}D_{y}^{b,p}\right)/R_{l}^{b,p}}{(\delta y)_{n}}, \quad \text{(A12e)}$$

$$d_{l}={}_{l}c_{p}^{l}\theta_{b,p}\Delta x\Delta y. \quad \text{(A12f)}$$

Appendix II. Interface Diffusion Coefficients

As illustrated in Fig. 3, grid points are always placed at the center of the control volumes. Therefore, when the control volume sizes are not uniform, their faces not lie midway between adjacent grid points. In these circumstances, Eq. (A13) can be used as the effective diffusion coefficient through the interface of the fracture and the matrix.

$$D_{f\to p}=\left(\frac{1-(\delta x)_{e+}/(\delta x)_{e}}{D_{T}}+\frac{(\delta x)_{e+}/(\delta x)_{e}}{\left(\theta_{p}D_{x}^{p}\right)}\right)^{-1} \quad \text{(A13)}$$

where the distances are defined in Fig. 4(b).

Similarly, the effective diffusion coefficient through the interface of the buffer and the matrix and the buffer and the fracture can be represented as Eqs. (A14) and (A15), respectively.

$$D_{b\to p}=\left(\frac{1-(\delta y)_{s+}/(\delta y)_{s}}{\left(\theta_{b}D_{y}^{b}\right)}+\frac{(\delta y)_{s+}/(\delta y)_{s}}{\left(\theta_{p}D_{y}^{p}\right)}\right)^{-1} \quad \text{(A14)}$$

and

$$D_{b\to f}=\left(\frac{1-(\delta y)_{s+}/(\delta y)_{s}}{\left(\theta_{b}D_{y}^{b}\right)}+\frac{(\delta y)_{s+}/(\delta y)_{s}}{D_{L}}\right)^{-1}. \quad \text{(A15)}$$

The interface diffusion coefficients, $D_{f\to p}$ should be the values replaced by $(\theta_{p}D_{y}^{p})$ in Eq. (A12) and (D_{T}) in Eq. (A10); in the same way, $D_{b\to p}$ replaced by $(\theta_{p}D_{y}^{b})$ in Eq. (A12) and $(\theta_{p}D_{y}^{p})$ in Eq. (A12), and $D_{b\to f}$ replaced by $(\theta_{p}D_{y}^{b})$ in Eq. (A12) and (D_{L}) in Eq. (A10).

References

1. Chiou, S.L. and S.H. Li., "Migration of Radionuclides in Fractured Porous Rock: Analytical Solution for a Flux-type Boundary Condition," *Nucl. Tech.*, **101**, 92-100, (1993).
2. Final Storage of Spent Fuel-KBS-3, SKBF/KBS Report, Stockholm (1983).
3. Green, J.S., Calculation of the Time Responses of Linear Systems, Ph.D. Thesis, University of London, (1955).
4. Lee, Y.M. *et al.*, "A Numerical Model for Nuclide Migration in the Far-field of the Repository," *J. Korean Nucl. Soc.*, **21**(4), 267 (1989).
5. Lee, Y.M. *et al.*, "Continuous Time Markov Process Model for Nuclide Decay Chain Transport in the Fractured Rock Medium," *J. Korean Nucl. Soc.*, **25**(4), 539 (1993).
6. Lee, Y.M. *et al.*, "A Stochastic Compartment Model for Nuclide Transport in the Fractured Porous Rock," Proc. of WM95, February 26-March 2, 1995, Tucson, Arizona, U.S.A. (1995).
7. Lee, Y.M. and K.J. Lee, "Nuclide Transport of Decay Chain in the Fractured Rock Medium: a

Model Using Continuous Time Markov Process," *Ann. Nucl. Energy*, **22**(2), 71 (1995).

8. Lee, Y.M. *et al.*, "A nuclide Transfer Model for Barriers of the Seabed Repository Using Response Function," *J. Korean Nucl. Soc.*, **28**(2), 539 (1996).
9. Lee, Y.M. and C.H. Kang, "A Method of Characteristics Solution of Nuclide Transport with Decay Chain," Proc. MRS' 97: International Symposium on the Scientific Basis for Nuclear Waste Management, Sept. 28-Oct. 3, 1997, Davos, Switzerland (1997).
10. Lee, Y.M. *et al.*, "A Nuclide Decay Chain Transport Model by the Method of Characteristics," J. Korean Nucl. Soc., 29(4), 539 (1997).
11. Lee, Y.M. and C.H. Kang, "Two-dimensional Nuclide Decay Transport in a Fractured Porous Medium by a Control Volume Approach," *Ann. Nucl. Energy*, **26**(17), 1569(1999).
12. Patankar, S.V., Numerical Heat Transfer and Fluid Flow, Hemisphere, Washington, D.C., (1980).
13. Sudicky, E.A. and E.O. Frind, "Contaminant Transport in Fractured Porous Media: Analytical Solutions for a System of Parallel Fractures," *Water Resour. Res.*, **18**(6), 1634, (1982).
14. Sudicky, E.A. and E.O. Frind, "Contaminant Transport in Fractured Porous Media: Analytical Solution for a Two-Member Decay Chain in a Single Fracture," *Water Resour. Res.*, **20**(7), 1021, (1984).
15. Tang, D.H. *et al.*, "Contamination transport in fractured porous media : Analytical solution for a single fracture," *Water Resour. Res.*, **17**(3) 555-564, (1981).